Monthly Notices of the ROYAL ASTRONOMICAL SOCIETY

MNRAS **527,** 6722–6731 (2024) https://doi.org/10.1093/mnras/stad3584
Advance Access publication 2023 November 21

# SDSS-IV MaNGA: the role of the environment in AGN triggering

Sandro B. Rembold,[1,2]★ Rogério Riffel ,[2,3,4]★ Rogemar A. Riffel ,[1,2] Thaisa Storchi-Bergmann,[2,4] Jaderson da S. Schimoia,[1,2] Greique A. Valk,[1,2] Vanessa Lorenzoni ,[1] Gabriele S. Ilha [1,5] and Luiz N. da Costa[2]

[1]*Departamento de Física, Centro de Ciências Naturais e Exatas, Universidade Federal de Santa Maria, 97105-900, Santa Maria, RS, Brazil*
[2]*Laboratório Interinstitucional de e-Astronomia – LIneA, Av. Pastor Martin Luther King Jr, 126 - Del Castilho, Nova América Offices, Tower 3000 / Room 817, Rio de Janeiro, RJ – 20765-000, Brazil*
[3]*Instituto de Astrofísica de Canarias, Calle Vía Láctea s/n, E-38205 La Laguna, Tenerife, Spain*
[4]*Departamento de Astronomia, Instituto de Física, Universidade Federal do Rio Grande do Sul, CP 15051, 91501-970, Porto Alegre, RS, Brazil*
[5]*Universidade de São Paulo, Instituto de Astronomia, Geofísica e Ciências Atmosféricas, Rua do Matão 1226, São Paulo, SP, 05508-090, Brazil*

Accepted 2023 November 17. Received 2023 November 15; in original form 2023 August 20

## ABSTRACT

The large- and small-scale environments around optically-selected AGN host galaxies and a control sample of non-active galaxies in the MaNGA survey have been investigated in order to evaluate the importance of the environment in AGN triggering. Using the MaNGA integral field spectroscopy, we quantify non-circular motions of the ionized gas and detect an excess of radial gas motions in AGN hosts relative to control galaxies, not associated to AGN feedback and are most likely the result of tidal interactions, possibly associated with the triggering of the AGN. We find that the large-scale environments are similar for the AGN hosts and control galaxies in our sample and are biased towards lower large-scale densities and group virial masses, suggestive that the large-scale environment properties is only relevant to the AGN phenomenon in an indirect way, in the form, e.g. of the morphology-density relation. The small-scale environment, as measured by the frequency and luminosity of close neighbours, was also found to be similar for AGN and control galaxies. However, we find a correlation between the intensity of the non-circular gas motions in AGN hosts and the strength of the tidal field, while the control sample does not present such correlation. Also, AGN hosts with the most intense radial gas motions present larger tidal fields than their control galaxies. These findings indicate that at least a fraction of the AGN hosts in our sample have been triggered by tidal interactions with nearby galaxies.

**Key words:** galaxies: active – galaxies: evolution – galaxies: groups: general.

## 1 INTRODUCTION

The triggering of nuclear activity requires the transport of significant amounts of matter towards the central regions of galaxies, which eventually results in accretion by a Supermassive Black Hole (SMBH). Such gas inflows involve an efficient mechanism of angular momentum dissipation of the gas in the galaxy (see Storchi-Bergmann & Schnorr-Müller 2019, for a comprehensive review). It has long been thought that this inflowing gas can originate from environmentally-driven mechanisms like merging or tidal interactions (e.g. Osterbrock 1993). Theoretical works have shown that the merging between two gas-rich galaxies can result in efficient angular momentum dissipation of the gas phase, followed by increased star formation rates and eventually feeding the SMBH (Barnes & Hernquist 1991; Kauffmann & Haehnelt 2000; Byrne-Mamahit et al. 2023). A similar process can result from less catastrophic tidal interactions (e.g. Noguchi 1988). Galaxy interaction may be a necessary ingredient to explain the AGN activity at least in the high-luminosity regime (Menci et al. 2014).

Observational studies conducted, especially in the last decades, have revealed hints about such AGN-environment relation. At the largest scales, an overall decrease in the incidence of optical and X-ray AGN is observed in the central regions of massive groups (Lopes, Ribeiro & Rembold 2017; Koulouridis et al. 2018), which has been interpreted as a result of the reduction in the availability of cold gas due to effects like ram-pressure stripping (Gordon et al. 2018). The low-density outskirts of groups seem to be more favourable to the occurrence of nuclear activity (Gordon et al. 2018), possibly a consequence of a larger cold gas reservoir combined with lower relative speeds between galaxies (Kim, Choi & Kim 2020). Interestingly, the void environment seems also to enhance the AGN activity (Ceccarelli, Duplancic & Garcia Lambas 2022).

At smaller scales, it has been observed that nuclear activity is also more common in the presence of close neighbours (Alonso et al. 2007; Rogers et al. 2009; Khabiboulline et al. 2014; Duplancic et al. 2021) compared to galaxies in groups. Ellison et al. (2011) found that this increase is more intense when the close companion has a comparable mass to the AGN host. Also, the SMBH accretion seems to be enhanced in pairs (Liu, Shen & Strauss 2012) relative to isolated galaxies. The fraction of AGN pairs was found to be higher than that expected from a random distribution (Ellison et al. 2011; Liu, Shen & Strauss 2012), and this fraction increases for smaller

★ E-mail: sandro.rembold@ufsm.br (SBR); riffel@ufrgs.br (RR)

separations between the pair members (Fu et al. 2018), suggesting a mutual triggering of AGN activity. Morphological signals of merging and tidal interactions also seem to increase the frequency of AGN (Alonso et al. 2007). Objects with post-merger morphologies are also more likely to harbour an AGN (Li et al. 2023) than normal galaxies. At higher redshifts, QSOs were also found to be more asymmetric, hinting at a merger-induced activity (Araujo et al. 2023).

There are, however, a number of works that challenge the above findings. Some authors have not found differences in the AGN fraction for galaxies with close neighbours relative to isolated ones (Schmitt 2001; Manzer & De Robertis 2014). Coldwell & Lambas (2006) have found no differences between the mean environments of QUASARs/Seyferts and non-active galaxies. No enhancement in AGN activity in pairs of merging galaxies has been found by Darg et al. (2010). Also, no increase in AGN activity in merging systems was found by Silva et al. (2021). Such different results may originate in the AGN definition and, crucially, from what kind of objects the AGN hosts are compared with. Also, most of these works rely on the calculation of the relative frequencies of AGN hosts and non-active galaxies across diverse environments; the AGN triggered by gas inflows due to tidal interactions is then extrapolated from such frequencies. The reason behind this strategy is that, for the large samples necessary for such kind of investigation, most of the available data are in the form of imaging plus single-slit spectroscopy. Such data do not allow a characterization of the gas physics associated with the AGN triggered by tidal interactions. Instead, this characterization can be achieved with integral field spectroscopy, for one can (at least potentially) observe the effects of the environment as they act on the galaxy in the form of kinematical disturbances in the gas of the AGN host, for example. In order to better understand the effects of the environment on AGN activity, it is important to detect the putative gas inflows that are ultimately due to the interaction of the AGN host with its environment.

The MaNGA optical integral field spectroscopic survey is an invaluable tool for this investigation. In Rembold et al. (2017), we have defined a sample of optically-selected AGN hosts and a control sample of inactive galaxies in the MaNGA survey. The properties of the stellar populations of AGN hosts and control galaxies have been investigated in Mallmann et al. (2018) and Riffel et al. (2023), and their gas and stellar kinematics were mapped in Ilha et al. (2019). In do Nascimento et al. (2019) and do Nascimento et al. (2022), the gas excitation, star formation rates, and gas-phase metallicities have been derived and compared between AGN and control galaxies, and the extension of the narrow-line region (NLR) and the inner, kinematically disturbed region of AGNs were obtained in Deconto-Machado et al. (2022). In Riffel et al. (2021), we presented a comparison between star-formation rate surface densities obtained from spectral synthesis of the stellar population and from the H$\alpha$ gas emission. In this paper, our goal is to map the occurrence of non-circular gas motions that can be associated with AGN triggering using the MaNGA data and characterize the environment of AGN hosts.

This paper is organized as follows: in Section 2, we describe the MaNGA spectroscopic observations, the sample of AGN hosts and control galaxies, and the methodology for quantifying both the environment and non-circular gas motions in the galaxies of our sample; the results are presented in Section 3. Our discussions and conclusions are presented in Sections 4 and 5. Throughout the paper, we assume a $\Lambda$CDM cosmology with $H_0 = 70\,\mathrm{km\,s^{-1}\,Mpc^{-1}}$, $\Omega_\mathrm{m} = 0.27$, and $\Omega_\Lambda = 0.73$.

## 2 DATA AND METHODS

### 2.1 AGN hosts and control sample

We investigate and compare the spatially-resolved gas kinematics of a sample of AGN hosts and a sample of non-active galaxies drawn from the SDSS-IV Mapping Nearby Galaxies at Apache Point Observatory (MaNGA) survey (Bundy et al. 2015). The MaNGA survey comprises integral field unit (IFU) optical spectroscopic observations in the range 3600–10 400 Å, with a resolution $R \sim 2000$ (Yan et al. 2016), for ∼10 000 nearby ($z \sim 0.03$) galaxies. Galaxies observed in the MaNGA survey are split between 'primary' and 'secondary' samples according to the extension of the galaxy covered by the IFU (1.5 and 2.5 effective radii, respectively; Wake et al. 2017). Each IFU is comprised of a fiber bundle containing from 19 to 127 fibers, with diameters ranging from 12 to 32 arcsec (Drory et al. 2015).

In this work, we use a sample of AGN hosts optically identified in the MaNGA survey following the methodology proposed by Rembold et al. (2017) and expanded to the complete MaNGA survey in Riffel et al. (2023). In short, we cross-match the MaNGA galaxy sample with the spectroscopic sample of the SDSS-III DR12 (Alam et al. 2015). Galaxies are then classified according to the optical emission-line ionization source using line measurements from Thomas et al. (2013) and a combination of the BPT (Baldwin, Phillips & Terlevich 1981) and WHAN (Cid Fernandes et al. 2010) diagnostic diagrams. Confirmed optical AGN hosts are located simultaneously in the Seyfert/LINER region of both the BPT and the WHAN diagrams. With this methodology, we obtain a sample of 298 confirmed optical AGN hosts in MaNGA.

Non-active control galaxies with similar redshifts, stellar masses, and morphologies as the AGN sample were then selected as a control sample (hereafter, CTL). This was made by selecting from the MaNGA survey: (a) galaxies that do not present detectable emission lines in their SDSS-III single-fiber spectra, (b) galaxies in the star-forming region of the BPT diagram, and (c) galaxies in other regions of the BPT diagram, on the condition that the WHAN diagram discards ionization from an AGN. A subsample of candidate control galaxies matching the redshifts and stellar masses of the confirmed AGN hosts at less than 30 per cent deviation was then selected. After visual inspection, we select the two objects that best match the morphology and projected axis ratio of the AGN host as their control 'partners'. Our final sample is composed of 293 AGN hosts[1] paired with 492 unique non-active galaxies.[2] We refer to Riffel et al. (2023) for a complete description of the AGN and control samples.

### 2.2 MEGACUBES

The characterization of the ionized gas kinematics of the AGN and control samples was performed using the emission-line fits derived by Riffel et al. (2023). The properties of all emission lines for a given galaxy, as well as the spaxel-by-spaxel properties of its stellar

[1]For five AGN hosts, no control galaxies were selected due to their location on the borders of the redshift-stellar mass space or the presence of morphological features that were not found elsewhere in the MaNGA survey; we do not discuss such objects further in the paper.

[2]This is less than the expected 586 control objects due to a number of occurrences where a given control galaxy was paired with more than one AGN host.

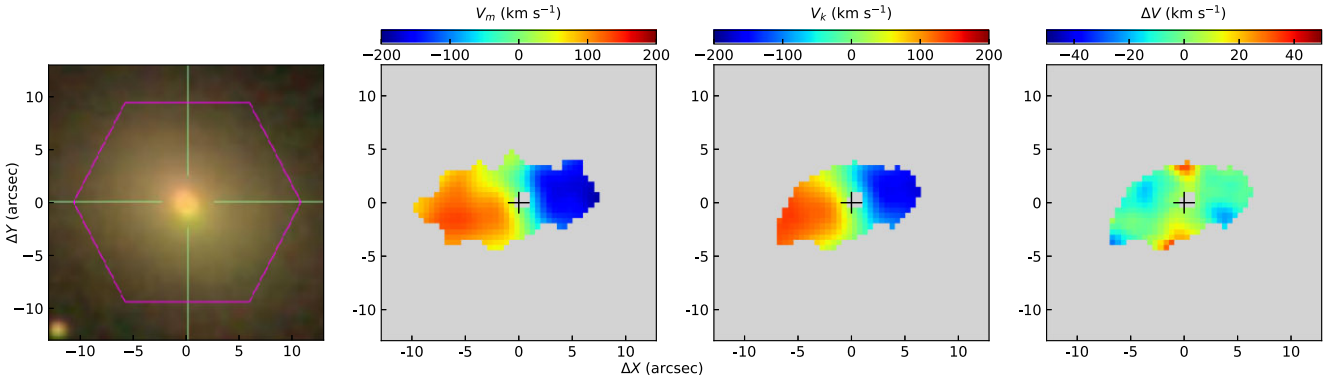


**Figure 1.** Example of kinematic modelling for the AGN host MaNGA-ID 1–37036. From left to right: the SDSS-III optical image of the galaxy including the borders of the MaNGA IFU data cube; the measured velocity map $V_m$ of H$\alpha$; the rotation model $V_k$ obtained with KINEMETRY; and the map of residuals $\Delta V = V_m - V_k$.

populations, are encapsulated in a single FITS volume referred to as MEGACUBE.[3]

The construction of the MEGACUBES was performed using the URUTAU (Mallmann & Riffel 2023) code[4], as folows. Each spaxel was corrected for Galactic reddening using the Schlegel, Finkbeiner & Davis (1998) extinction maps, and the Cardelli, Clayton & Mathis (1989) reddening law. The spectra were then corrected to restframe using the SDSS-III redshift values available in the drpall tables of the MaNGA data base. The spectral continuum for each spaxel was modelled via full spectral fitting stellar population synthesis using the STARLIGHT[5] fitting code (Cid Fernandes et al. 2005; Cid Fernandes 2018) and a grid of 84 single stellar populations based on the Miles (Vazdekis et al. 2010) and González Delgado et al. (2005) models updated with the Miles V11 models (Vazdekis et al. 2016), with stellar ages spanning from 0.001 to 12.6 Gyr and metallicities $Z$ from 0.19 to 1.66 $Z_\odot$, including a power law of the form $F_\nu \propto \nu^{-1.5}$ to account for the contribution of a possible AGN continuum (see Riffel et al. 2021, 2023, for a complete description). Fluxes and equivalent widths of the most common emission lines were then measured on the residual spectra (observed minus synthetic) using the IFSCUBE[6] PYTHON package (Mallmann & Riffel 2020; Ruschel-Dutra et al. 2021). The line profiles are fitted with Gaussian functions. In order to reduce the number of free parameters and reduce overfitting, the width and centroid velocities of emission lines from the same parent ion were fixed to the same value and the [O III]λ5007/λ4959 and [N II]λ6583/λ6548 flux ratios were fixed to their theoretical values of 2.98 and 3.06, respectively.

In this work, we use only the derived properties of the H$\beta$, [O III]λ5007, H$\alpha$, and [N II]λ6583 emission lines to map the gas ionization and kinematics.

### 2.3 Modelling non-circular motions

One of our goals is to detect and quantify non-circular gas motions that can be linked to the feeding of the SMBH. In AGN hosts, deviations from strict circular motion in the ionized gas can also be due to outflows. Previous works involving MaNGA data have indeed shown that the gas kinematics are distinct between AGN and non-active galaxies in regions close to the galaxy centre (Ilha et al. 2019; Deconto-Machado et al. 2022). Discriminating between inflows and outflows is possible when performing detailed, individual analyses of the spatially-resolved ionization profiles and gas kinematics, but such methodology is unfeasible in an automated fashion for large samples. However, it has been observed that the kinematically-disturbed region around AGN associated with outflows presents a less extended distribution than that of the extended narrow-line region (ENLR – Fischer et al. 2018; Deconto-Machado et al. 2022). We therefore restrict the kinematic analysis of the ionized gas to regions beyond the ENLR, i.e. to spaxels where the optical emission lines do not have an active nucleus as the main ionization source. In practice, we replicate the same technique used in the definition of the control sample by Rembold et al. (2017): all spaxels that are confirmed as AGN by both diagnostic diagrams (BPT and WHAN), as well as those in the Transition region, are removed from the spatially-resolved velocity maps for all galaxies in our sample.

The modelling of the gas kinematics was performed using the KINEMETRY code (Krajnović et al. 2006). KINEMETRY performs a kinematic modelling of the spatially-resolved line-of-sight velocity distribution in elliptical annuli around the nucleus of the galaxy. For each annulus, the best-fit coefficients of a harmonic expansion of the velocity distribution are obtained. We have run KINEMETRY to produce a rotation model of the ionized gas as traced by the H$\alpha$ emission line, excluding those spaxels whose ionization is dominated by the AGN and spaxels in the Transition region of the BPT diagram. Prior to the fits, we smooth the velocity maps for each emission line using a Gaussian kernel with $\sigma = 1.5$ pixels to reduce the pixel-to-pixel variations in the velocity due to noise and remove all isolated spaxels (those containing less than four adjacent spaxels). As a final smoothing step, we compare the H$\alpha$ velocity of each spaxel to the average velocity $\bar{v}_{30}$ of its 30 nearest neighbour spaxels; for all those spaxels whose velocity deviates more than 3.5$\sigma$ from $\bar{v}_{30}$, we iteratively replace its velocity by $\bar{v}_{30}$. In the fitting process, the kinematic centre was fixed to the location corresponding to the peak of the continuum emission, derived from the best-fit STARLIGHT solution. We also limit the kinematic modelling to elliptical regions with a minimum cover factor (i.e. the fraction of valid pixels along the fitted ellipse at any given radius) of 0.9. We perform the kinematic modelling using only the H$\alpha$ line, for it is one of the most prominent lines in our spectra.

Fig. 1 shows the velocity distribution and the kinematic modelling of the H$\alpha$ line obtained with KINEMETRY for galaxy MaNGA-ID 1–37036, a confirmed AGN host. Notice the lack of velocity information in the central region, where ionization from the AGN is dominant. The kinematics of the H$\alpha$-emitting gas is dominated by rotation,

[3]All MEGACUBES are available at https://manga.linea.org.br/.
[4]https://github.com/ndmallmann/urutau
[5]http://www.starlight.ufsc.br/
[6]https://github.com/danielrd6/ifscube

but there are clear departures from simple rotation, as evident in the residual map obtained by subtracting the modelled rotation velocities from the observed ones. These residuals may be associated to inflows or to disturbances in the gas kinematics due e.g. to interactions.

In order to encapsulate the occurrence and intensity of radial gas motions in the residual velocity maps in a single numerical parameter, we calculate the average absolute value of the residual velocity map, $\langle \Delta V \rangle$, i. e.

$$\langle \Delta V \rangle = \frac{1}{N} \sum_{i}^{N} |V_{\mathrm{m},i} - V_{\mathrm{k},i}|, \quad (1)$$

where $V_{\mathrm{m},i}$ and $V_{\mathrm{k},i}$ are the measured gas velocity and the model rotation velocity obtained from KINEMETRY for spaxel $i$, and $N$ is the number of spaxels contained in the model. Being an averaged quantity, $\langle \Delta V \rangle$ is sensitive to the relative importance of the structures found in the residual maps, be it due to large offsets between the measured and modelled gas velocities or to structures that occupy a large fraction of the galaxies' physical extensions. Because $\langle \Delta V \rangle$ is strictly non-negative, a certain level of bias due to noise is expected. However, possible systematic differences in $\langle \Delta V \rangle$ between AGN and non-active control galaxies are independent of such bias, so we do not introduce any kind of correction due to this effect.

### 2.4 Environment characterization

We have characterized the properties of the environment around the galaxies in our sample at 'large' ($\gtrsim$1 Mpc) and 'small' ($\lesssim$100 kpc) physical scales.

At large scales, we characterize the galaxy environment through its membership or not to a group or cluster of galaxies, the mass of such system and the numerical density of bright galaxies at such physical scales. This can be accomplished by cross-matching the objects in our sample with a catalogue of groups[7] of galaxies and isolated objects. For this goal, we have used the group catalogue presented by Tempel et al. (2017). This catalogue is based on the SDSS-III spectroscopic data base and therefore includes a large fraction of the galaxies in our sample, even though it does not include the entire footprint of the SDSS-III. Groups have been identified in the projected position – redshift space with the friends-of-friends technique. Galaxies not associated with any structure are considered as isolated objects. For each group, the virial mass $M_{200}$ is estimated, and the luminosity rank of the galaxy in the system is also determined. For both isolated and group galaxies, the local galaxy density at four different scales, from 1.5 to 10.0 Mpc, is also derived. Notice that this density estimation is based on the spectroscopic sample of the SDSS-III survey, and therefore includes mostly bright ($m_r < 17.77$) galaxies. The catalogue contains 88 662 galaxy groups with two or more confirmed members.

After performing the cross-match between this catalogue and our samples of AGN hosts and non-active control galaxies, we find 655 objects in common. For those objects, we extract galaxy membership, parent halo mass, and luminosity rank (when available) and the local galaxy density; no significant differences were found when using the different density estimators, so in the following, we present only the results for the density at the 1.5 Mpc scale.

In order to map the galaxies' environments at smaller scales, we determine the number of close neighbours inside a fixed radius around each galaxy in our sample. This differs from the density estimator above in several aspects. The first is the physical scale: we restrict the search radius to a 100 kpc scale around each galaxy. Secondly, we do not restrict ourselves to the spectroscopic sample of the SDSS-III, but rely also in the photometric source catalogue for those sources classified as extended (galaxies) and for which a photometric redshift was estimated. This results in the inclusion of a large number of faint sources that are not present in the spectroscopic sample. Using the CASJOBS[8] environment, we select as probable neighbours of a galaxy all extended sources whose photometric redshifts are compatible with the spectroscopic redshift of the galaxy given their uncertainties. Because the uncertainties in the photometric redshift estimations are usually large, a fraction of these objects may in fact include foreground or background sources. However, this contamination is expected to be present both in the AGN and control samples, so the exact number of confirmed members is not relevant to our analysis. It is important to notice that, while the large-scale environment parameters can be easily drawn from the Tempel et al. (2017) catalogue, the close neighbour counts have to be determined individually; for this reason, we compare the properties of AGN hosts and CTL galaxies with those of the complete MaNGA sample only using the large-scale environmental parameters.

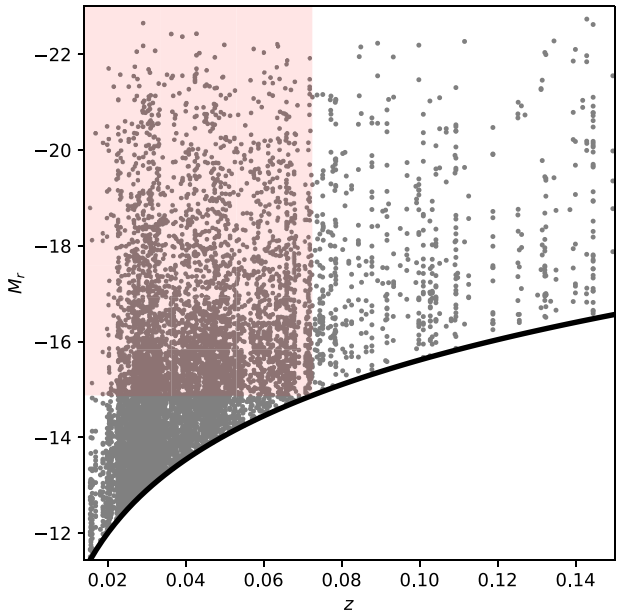


**Figure 2.** Photometrically identified close neighbours (grey circles) with $M_r < -14.87$ mag as a function of their luminosity and redshift of the parent AGN host/CTL galaxy. The red box indicates the redshift and absolute magnitude limits of our complete sub-sample of neighbours.

The photometric sample of the SDSS-III is complete up to $m_r = 22.7$ mag, but becomes increasingly incomplete for fainter sources. Therefore, the number of photometric neighbours for a galaxy varies strongly with redshift. In order to guarantee the largest possible complete sample of photometric neighbours for the galaxies in our sample, we limit our analysis to galaxies below the 90 per cent percentile of the redshift distribution (i.e. galaxies with $z \lesssim 0.073$). We also limit our analysis to a volume-limited sample of photometric neighbours brighter than the absolute magnitude corresponding to the photometric completeness limit ($m_r = 22.7$ mag) at this redshift, or $M_r < -14.87$ mag. Fig. 2 shows the absolute magnitudes $M_r$ of all photometrically identified neighbours of the galaxies in our

[7]In this paper, the term 'group' refers to groups and clusters of galaxies irrespective of richness or mass.

[8]https://skyserver.sdss.org/casjobs/

sample brighter than $m_r = 22.7$ mag, and the neighbours included in the volume-limited sample. The magnitude cut $M_r = -14.87$ corresponds to faint objects like the Small Magellanic Cloud, so we are probing all the way from the mass scale of the largest satellites of Milky-Way-like galaxies to objects brighter than the AGN hosts and control galaxies in our sample.

Having determined the volume-limited sample of photometric neighbours, we calculate for each galaxy in our sample the tidal parameter $Q$ (Verley et al. 2007; Argudo-Fernández et al. 2015), defined by

$$Q = \log \sum_{i}^{N} \frac{M_i}{M} \left(\frac{R}{d_i}\right)^3, \quad (2)$$

where $M_i$ is the mass of the $i$-th neighbour, $d_i$ its projected distance to the galaxy, $M$ is the mass of the galaxy, and $R$ its radius. Large values of $Q$ are expected to be associated with galaxies subject to potentially more intense tidal fields. It is important to notice that the above definition for the tidal parameter does not take explicitly into account the line-of-sight distances between a galaxy and its putative neighbours. Including in the calculation of $Q$ only candidate neighbours that are also close to the main galaxy in redshift space (and therefore are more likely to be gravitationally bound to it) is an important step, but it does not guarantee a perfect assessment of the tidal field strength due to the fact that the non-cosmological component of the observed redshift of a galaxy pair cannot be translated into a distance measurement between the galaxies of the pair along the line of sight. This is true when using either spectroscopic or photometric redshifts, but is especially dramatic with photometric redshifts due to their much larger uncertainties. Therefore, the values of $Q$ derived by us are meaningful only in a statistical sense.

For the calculation of $Q$, we use the effective radius $R_e$ obtained from the NASA-Sloan Atlas as a proxy for the radius of the galaxy. Also, the relative masses of the parent galaxy and their satellites were estimated from the ratio of their $r$-band luminosities. The use of the $r$-band luminosity as a proxy for dynamical mass assumes implicitly that all neighbours follow the same mass-to-light ratio $M/L_r$ as their parent galaxy, an assumption that is most likely incorrect in general. We highlight, however, that our aim is to detect possible systematic differences between AGN and CTL galaxies; the errors introduced in the calculation of $Q$ due both to the assumption of a fixed $M/L_r$ and to the use of photometric redshifts to identify potential close neighbours do not bias one sample relative to the other and are therefore not expected to affect our results significantly.

## 3 RESULTS

### 3.1 The large-scale environment of AGN and CTL galaxies

As a first characterization of the large-scale environments of AGN and CTL galaxies, we separate all sources in our sample between isolated objects and those that are associated to groups of galaxies. Most of the galaxies in our sample are isolated objects, and only a handful of the remaining ones are associated to very rich clusters, which makes a direct comparison between the richness distributions difficult. In order to simplify the analysis of the environment of AGN and CTL galaxies, we split the group sample into 'rich' (those groups containing more than six spectroscopically confirmed members) and 'poor' groups (the remaining ones). Fig. 3 presents the relative fractions of isolated galaxies and those in poor/rich groups for the AGN hosts and CTL galaxies. We also present the distributions for

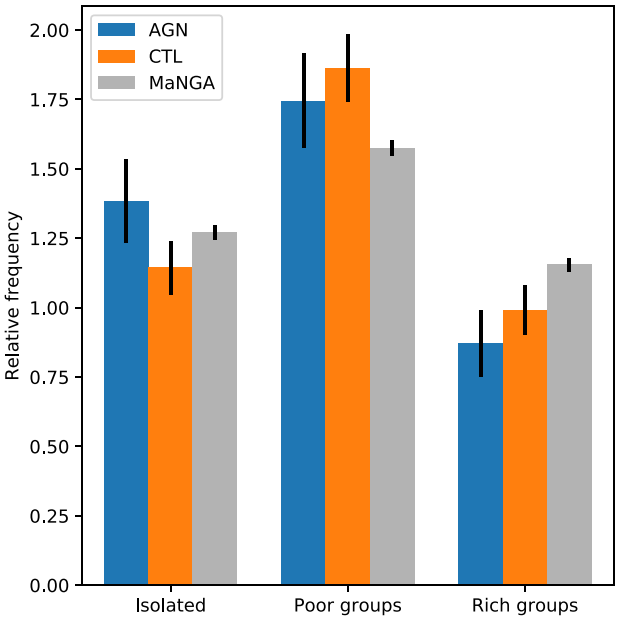


**Figure 3.** Distribution of large-scale environments (isolated galaxies and those in poor/rich groups) for AGN and CTL galaxies. The error bars are estimated from a Poisson distribution.

the complete MaNGA sample. The distribution for CTL galaxies is very similar to that of the AGN sample, but the AGN sample presents a slight excess of isolated galaxies with relation to CTL galaxies; the raw counts in each category are compatible with them being drawn from the same parent distribution, however. Compared with the complete MaNGA sample, the AGN sample (and the CTL sample to a lesser degree) seems to avoid the environment of rich groups.

The above tendency is confirmed in panel (a) of Fig. 4, where we plot the distributions of the local galaxy density at a 1.5 Mpc scale, $\rho_{1.5}$. Compared to the complete MaNGA sample, both AGN and CTL galaxies are biased towards lower environmental densities. The Kolmogorov–Smirnov (KS) test confirms that these distributions are not drawn from the same parent distribution at $10\sigma$ significance. The differences between the distributions of AGN and CTL galaxies, on the other hand, are not statistically significant ($p = 0.24$). Focusing on those galaxies that are confirmed members of groups, we present in Fig. 4 panel (b) the distribution of halo virial masses $M_{200}$. Once again, AGN hosts tend to be found in lower mass groups relative to the complete MaNGA sample at more than $10\sigma$ significance. A very discrete tendency for AGN hosts towards lower densities compared with the CTL galaxies is also observed, but it is not statistically significant ($p = 0.097$). This confirms that MaNGA AGN galaxies are more typically found in lower-density, low-mass environments. This tendency may be due to the need of a cold gas supply in order to feed the nuclear activity in a galaxy, while the high densities of rich groups tend to reduce the available cold gas reservoir and quench the star formation (Boselli & Gavazzi 2006).

In the panel (c) of Fig. 4, we present the distributions of absolute line-of-sight relative velocities $V_{LOS}$ in the restframe of the parent group of each galaxy in our sample normalized by the velocity dispersion $\sigma$ of the same group. We include only groups containing at least 3 members because, for a pair, $|V_{LOS}/\sigma| = 0.707$ by construction, resulting in a dominant 'peak' that makes a direct interpretation difficult. Minor differences are observed between AGN hosts and both CTL galaxies and the complete MaNGA sample; the KS test does not indicate any systematic trend. Finally, we compare

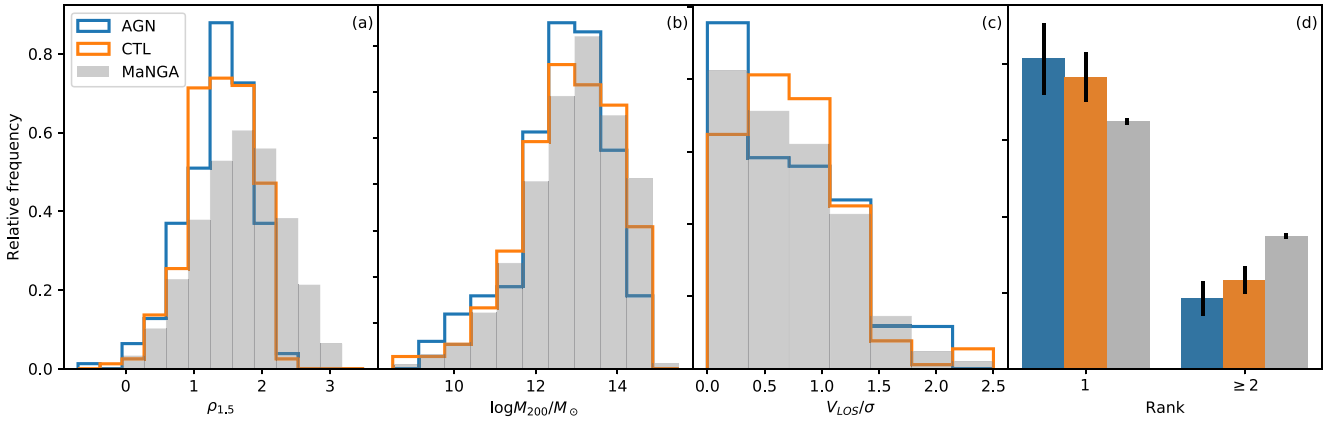


**Figure 4.** Distributions of (a) environmental densities at a scale 1.5 Mpc ($\rho_1$), (b) virial mass $M_{200}$ of the parent group, (c) absolute line-of-sight relative velocity $V_{\rm LOS}/\sigma$, and (d) luminosity rank (1 for brightest galaxy in the association or isolated galaxy, 2 otherwise) for AGN (blue) and CTL (orange) galaxies in our sample, as well as the respective distributions of the complete MaNGA sample (grey).

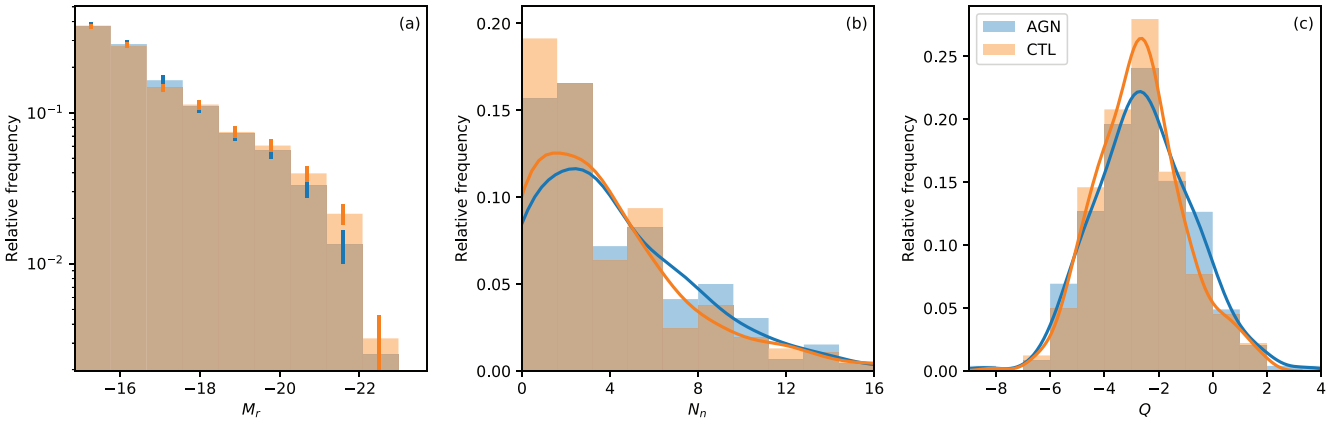


**Figure 5.** (a) *r*-band luminosity distribution of the close neighbours of the AGN and CTL samples. Error bars were estimated from a Poisson distribution. (b) Distributions of the number of close neighbours around AGN hosts and CTL galaxies in our sample. (c) Distributions of the tidal parameter $Q$ for AGN hosts and CTL galaxies. AGN hosts/CTL galaxies are represented by blue/orange shaded regions, respectively. The blue and orange lines in panels (b) and (c) represent a Gaussian kernel smoothing of the AGN and CTL distributions, respectively.

in Fig. 4 panel (d) the luminosity rank of the galaxy in the structure it resides. Isolated galaxies are included in this plot and, for such objects, the galaxy rank is 1 by definition. Compared to the complete MaNGA sample, AGN hosts (and CTL galaxies to a somewhat lesser degree) are more likely to be the first-ranked galaxy in the structure it resides. This may be due to a combination of the tendency of AGN hosts to avoid dense, high-mass structures and the fact that optical AGN are found more frequently in more massive galaxies (Kauffmann et al. 2003).

It is important to note that the environments of AGN and CTL galaxies are very similar, even though no information whatsoever regarding the environment of AGN hosts has been used as a reference when selecting the CTL sample. The fact that the CTL sample, selected taking into account only the AGN host stellar masses and morphologies, reproduces so well the environmental trends of AGNs is suggestive that the large-scale environment of the galaxy is not an important driver of their observed nuclear activity in a statistical sense.

### 3.2 Close neighbours of AGN and CTL galaxies

In Fig. 5, we present the global statistics of the population of close neighbours of our sample of AGN hosts and CTL galaxies. Panel (a) presents the luminosity function of the close neighbours for AGN hosts and CTL galaxies. As expected, the luminosity function is skewed towards low-luminosity objects. The distributions for AGN and CTL galaxies are very similar; for the largest luminosity bins, a slight excess is observed for CTL galaxies relative to AGN hosts, but this difference is not significant taking into account the uncertainties in the galaxy counts.

The distributions of the number of neighbours around each galaxy are presented in panel (b) of Fig. 5. Most galaxies in our sample contain at least one – and in general more than one – close neighbour. Once again, the distributions are very similar, and the $p$-value of the KS test (0.60) confirms that both are statistically indistinguishable. The same is true for the distributions of the tidal parameter $Q$, shown in panel (c) of Fig. 5: the tidal field around AGN and CTL galaxies is very similar, and the distributions of $Q$ are not statistically different ($p = 0.31$).

The above results show that the environment around AGN hosts is similar to that observed for CTL galaxies also at scales smaller than ∼100 kpc, at least regarding the number of close neighbours, their luminosities and the tidal field they produce.

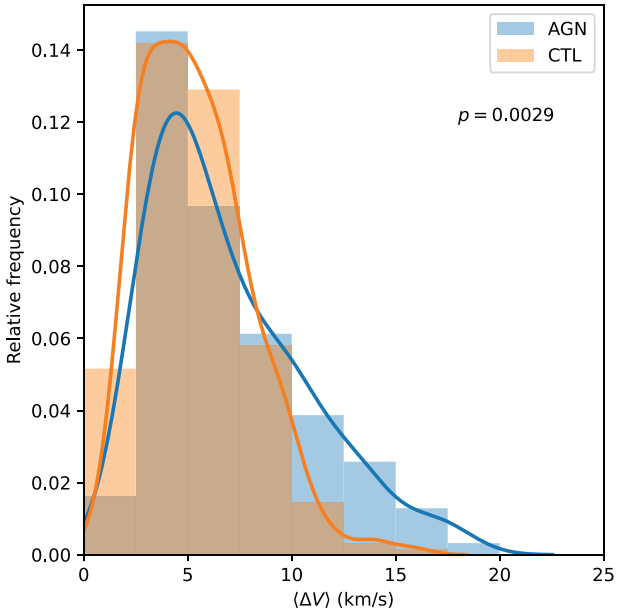


**Figure 6.** Distributions of $\langle \Delta V \rangle$ for AGN (blue shaded area) and CTL (orange shaded area) galaxies. As in Fig. 5, the blue and orange lines represent a Gaussian kernel smoothing of the AGN and CTL distributions, respectively; the crossing point of these lines occurs at $\langle \Delta V \rangle \sim 8.4\,\mathrm{km\,s^{-1}}$, above which the AGN distribution dominates.

### 3.3 Non-circular gas motions

Fig. 6 presents the distribution of the mean velocity excess $\langle \Delta V \rangle$ for our sample galaxies. A striking difference is observed in the sense that AGN hosts present, on average, consistently larger values of $\langle \Delta V \rangle$ than CTL galaxies at more than $3\sigma$ significance ($p = 0.0029$). This means that a larger contribution of non-circular gas motions is present in the AGN sample relative to the control one. The smoothed distributions overlap at $\langle \Delta V \rangle \sim 8.4\,\mathrm{km\,s^{-1}}$, above which the AGN hosts dominate.

In order to understand the origin of this excess in $\langle \Delta V \rangle$ for AGN hosts, we calculate separately the contribution of each annular region around the galaxy centre to the total $\langle \Delta V \rangle$, and then average these values across all AGN hosts. This calculation was performed only for annular regions, including at least 15 per cent per cent of the AGN sample; the resulting $\langle \Delta V \rangle(R)$ profile extends from roughly 0.4 to 1.6 $R_e$. The same calculation was performed for CTL objects. In order to allow a fair comparison between AGN and CTL galaxies, we include in the CTL profiles only the spaxels that extend between the inner and outer radial limits of the respective AGN profiles. Fig. 7 shows the average profiles for AGN and CTL galaxies. We observe an excess in $\langle \Delta V \rangle$ for AGN hosts across all radii, but the most significant differences occur in the inner $R < 0.5R_e$ region and in regions farthest than 1 $R_e$ from the galaxy nuclear region. We stress this fact because the number of spaxels at a given radial distance scales linearly with the radial distance, and therefore most of the signal to the total $\langle \Delta V \rangle$ comes from regions far from the nucleus of the galaxy. We therefore conclude that the main driver of the difference in $\langle \Delta V \rangle$ between AGN and CTL galaxies comes from regions beyond the AGN host effective radius.

We further investigate if the observed difference in $\langle \Delta V \rangle$ can be associated to the large-scale environment where the galaxy is located. Fig. 8 shows the average values of $\langle \Delta V \rangle$ for isolated galaxies and those in poor or rich groups. This figure shows that the excess in $\langle \Delta V \rangle$ observed for AGN hosts relative to CTL galaxies is observed across

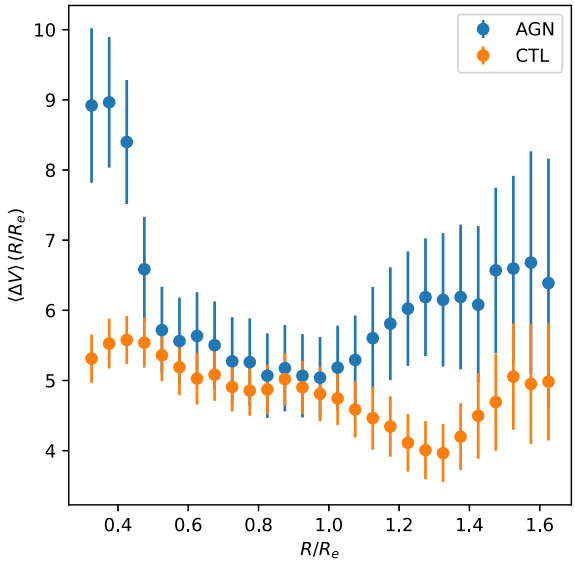


**Figure 7.** Radial distributions of the average $\langle \Delta V \rangle$ values for AGN (blue) and CTL (orange) samples. The error bars correspond to the standard error of the mean across all galaxies in each subsample.

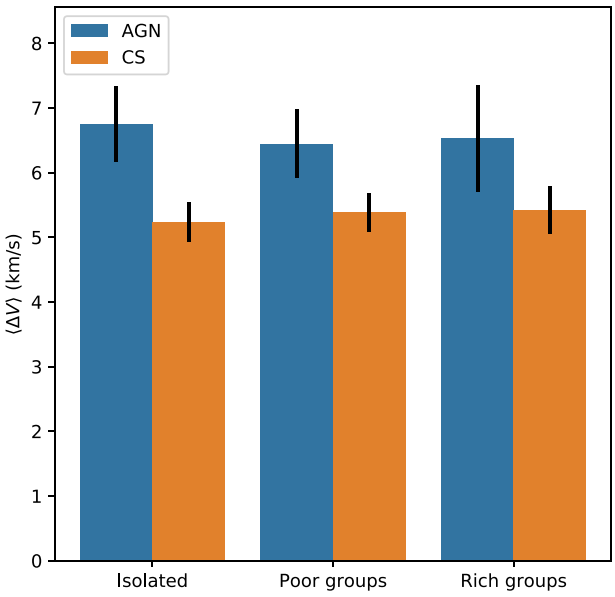


**Figure 8.** Average values of $\langle \Delta V \rangle$ for the galaxies in our sample separated in isolated galaxies and group members (both poor and rich). The error bars are estimated from a Poisson distribution.

all environments, from isolated galaxies to those in rich groups. We therefore conclude that the large-scale environment is not the main driver of the $\langle \Delta V \rangle$ excess in AGN hosts.

Finally, we check whether the local environmental properties can be responsible for the observed differences in $\langle \Delta V \rangle$. In Fig. 9, we plot the $\langle \Delta V \rangle$ values as a function of the tidal parameter $Q$. For CTL galaxies, we see no correlation whatsoever between $\langle \Delta V \rangle$ and $Q$. For the AGN hosts, however, the situation is radically distinct: $\langle \Delta V \rangle$ increases sharply as a function of $Q$, a tendency confirmed at almost $3\sigma$ with the Spearman correlation test ($p = 0.0072$). Both samples seem to be indistinguishable at the lower limit of $Q$, where $\langle \Delta V \rangle \sim 5\,\mathrm{km\,s^{-1}}$ for both AGN and CTL galaxies, but differences in $\langle \Delta V \rangle$ reach up to $\sim 4\,\mathrm{km\,s^{-1}}$ at the largest $Q$ values. This is

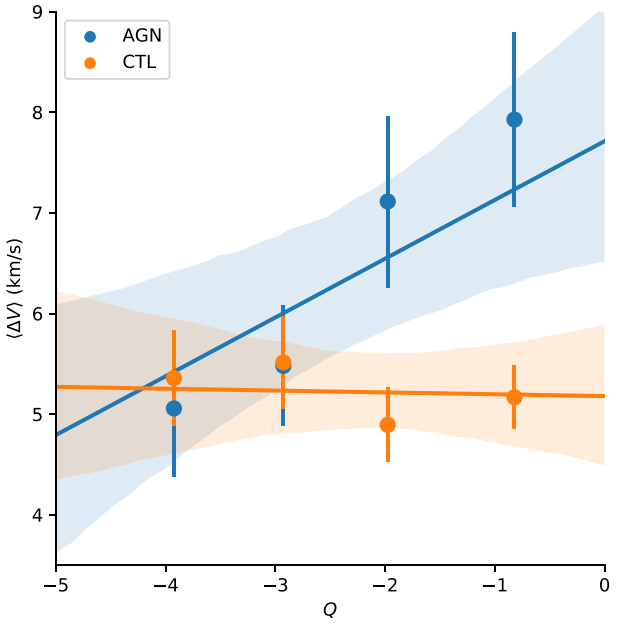


**Figure 9.** The dependence of $\langle \Delta V \rangle$ on the intensity of the tidal field as mapped by the tidal parameter $Q$. Average values of $\langle \Delta V \rangle$ across different bins in $Q$ are represented by blue (AGN) and orange (CTL) circles; the best-fit linear regression is shown by continuous lines, and the uncertainties are indicated by the shaded areas.

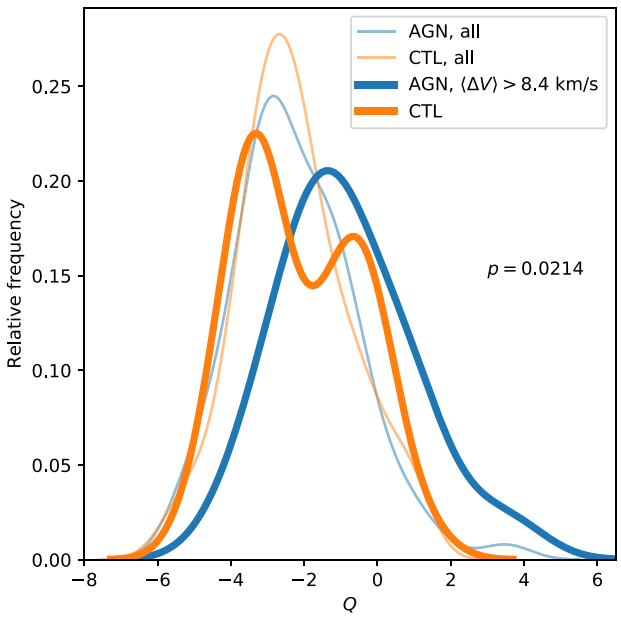


**Figure 10.** Distribution of the tidal parameter $Q$ for AGN (blue) and CTL (orange) galaxies. The thin lines represent the distributions of the complete AGN/CTL samples, as in Fig. 5; the thick lines represent the distributions of $Q$ for AGN hosts with $\langle \Delta V \rangle > 8.4\,\mathrm{km\,s^{-1}}$ and their respective CTL galaxies.

strongly suggestive of a connection between the occurrence of non-circular gas motions – what ultimately triggers the nuclear activity by bringing gas towards the inner regions of galaxies – and the tidal field of the immediate vicinity of a galaxy.

## 4 DISCUSSION

We have observed that the large-scale environmental properties of AGN hosts and CTL galaxies are both distinct from the complete MaNGA sample. These two subpopulations tend to be located in less dense regions, and when they are group members, the mass of the system tends to be lower. AGN hosts and CTL galaxies do, however, match their large-scale environmental properties. It is important to stress that no effort has been made to match the environments of AGN hosts and CTL galaxies when the CTL sample was defined. This means that a simple mass plus morphology selection biases the CTL of galaxies the same way as the AGN hosts regarding the large-scale environment, suggestive that the main driver of the differences between the environment of the AGN and the complete MaNGA sample is not directly related to nuclear activity but is instead due to the dependence of the galaxy morphology and mass on the environment.

The same seems to be true for the closer environment. We have not found differences in the tidal parameter $Q$ between AGN and CTL galaxies. This could suggest that even the small-scale environment around a galaxy is not related with nuclear activity. We have, however, found differences in the mean values of the non-circular velocity component $\langle \Delta V \rangle$. The fact that most of the signals that results in the observed differences in $\langle \Delta V \rangle$ come from regions far from the galaxy centre is suggestive that it is related to environment, e.g. through tidal interactions with neighbour galaxies. We have also shown that most of the differences in $\langle \Delta V \rangle$ come from galaxies with high $Q$ values, and that AGN and CTL galaxies are indistinguishable at low $Q$.

We can interpret these findings in a scenario where the local environment of a galaxy, as opposed to its large-scale environment, can trigger AGN activity. AGN and CTL galaxies are found in similar environments. The AGN phase in a galaxy can be triggered by secular processes like disc instabilities, which is likely the case for AGN hosts that present low $Q$ values. However, tidally-induced AGN are activated at large $Q$ values. This brings up the question of why the AGN hosts, and not the CTL galaxies, are sensitive to $Q$? In fact, the $Q$ values map the tidal field only in a statistical sense because, as discussed in Section 2.4, the distances of the neighbours to the parent galaxy are in fact a projected distance. Also, $Q$ does not discriminate the time evolution of the interaction, i.e. it is difficult to evaluate at what stage of the interaction between the parent galaxy and their neighbour objects are located. We have shown that AGN hosts seem to be more sensitive to the environment (in the sense that they present larger $\langle \Delta V \rangle$ values on average) at large $Q$, suggesting that AGN hosts have already had time to feel the effects of the tidal field. Such tidal interactions induce radial motions that eventually trigger the AGN and can still be detected at the active phase. In contrast, galaxies that are still not affected by the tidal field have become AGN by secular processes unrelated to the environment.

The above interpretation implies that galaxies subjected to more intense tidal fields are more likely to become active. One would therefore expect that a sample of AGN hosts, be it triggered by internal processes or tidally induced, are statistically more likely to present high $Q$ values relative to non-active galaxies. However, the distribution of $Q$ was found to be similar for AGN and CTL. On the other hand, we must take into account that $Q$ is subject to contaminants along the line of sight, so a large ammount of scattering is expected for galaxies that are subject to similar tidal fields. Ideally, we should compare the $Q$ values among active and control galaxies only for those AGN hosts that are in fact triggered by the tidal field, i.e. those presenting intense radial motions of the gas. We estimate from Fig. 6 that the excess in $\langle \Delta V \rangle$ for AGN relative to CTL galaxies becomes dominant at $\langle \Delta V \rangle \sim 8.4\,\mathrm{km\,s^{-1}}$. In Fig. 10, we

present the distributions of $Q$ for AGN hosts with $\langle \Delta V \rangle > 8.4\,\mathrm{km\,s^{-1}}$ compared to that of their own CTL galaxies. We show in the plot only a Gaussian kernel smoothing of the distributions for display purposes. The $Q$ distributions of the complete AGN and CTL samples are also shown for reference. The AGN with large $\langle \Delta V \rangle$ are indeed biased towards higher values of $Q$ relative to their CTL galaxies at more than $2\sigma$ significance ($p = 0.0214$). This difference disappears when we compare AGN hosts with CTL galaxies at low $\langle \Delta V \rangle$ values. We therefore conclude that interactions of a galaxy with their immediate vicinity can indeed induce non-radial gas motions that ultimately trigger nuclear activity.

Along similar lines, Raimundo, Malkan & Vestergaard (2023) have recently found increased AGN fractions in galaxies containing misalignments between the ionized gas and stellar kinematics relative to galaxies that do not display this feature. In order to explain this finding, the authors propose an external origin for the gas, like wet merging or direct gas capture from a nearby galaxy. In such events, inflowing gas reaches the innermost regions of the parent galaxy, triggering the AGN; the remaining gas assumes a rotational configuration distinct from the stellar kinematics of the parent galaxy. A similar mechanism may also play a role in the increased non-circular ionized gas motions observed in our AGN sample as compared to the CTL sample; in this case, however, the inflowing gas is still not settled in a purely rotational configuration – otherwise, no residuals in the ionized gas velocity field would be detected. Such mechanism is more likely to explain optical early-type AGN hosts, both because of the overall low-gas content of early-type galaxies in general (suggestive of gas accretion at later times), and because late-type galaxies are expected to efficiently dissipate the kinematics of external, infalling gas due to their own gas discs.

On the other hand, it has been found that type 2 quasars/QSOs are more asymmetric and/or show morphological features reminiscent of interactions; depending on the sample definition, such features are more likely associated with a post-coalescence (Araujo et al. 2023) or pre-coalescence phase (Pierce et al. 2023). Recent cosmological simulations (e.g. Singh et al. 2023) confirm that the close environment has an important role in funnelling the host gas towards the SMBH. This is suggestive that very luminous, optically-selected AGN can be triggered by close encounters or merging; given the high accretion rates associated to luminous optical AGN, a large supply of external gas (or an important kinematical disturbance in the gas of the host) is needed. By contrast, our sample of AGN is dominated by low-luminosity objects, indicative of lower accretion rates. For such objects, the SMBH triggering could in principle involve a much less extreme event, so that the AGN host can keep its overall morphology unchanged, while echoes of this event are still observable in the ionized gas velocity field. Interestingly, such environmental mechanisms may also play a role in SMBH feeding for active galaxies besides the ones identified in the optical. Mountrichas et al. (2023) have found that the star formation and nuclear activity in X-ray selected AGN can be induced by interactions. In the case of radio galaxies, Bernhard et al. (2022) have found that mergers are a viable triggering mechanism for AGN containing also strong optical lines. The close environment – and mechanisms like merging and tidal interactions – seems to be an important driver of AGN activity in general, nicely explaining our results.

## 5 CONCLUSIONS

We present an analysis of the large- and small-scale environments around optical AGN hosts and a control sample of non-active galaxies selected in the MaNGA survey. Non-circular motions of the ionized gas were quantified and confronted with the environmental properties of the galaxies, in order to identify signs of environmentally-triggered nuclear activity. Our main conclusions can be summarized as follows:

(i) The large-scale environments, as characterized by local densities at ∼1.5 Mpc scale, membership to a group of galaxies, and virial mass of the parent group, are similar for the AGN hosts and CTL galaxies in our sample. In contrast, the complete MaNGA sample is biased towards higher large-scale densities and group virial masses. This suggests that the large-scale environment properties are only relevant to the AGN phenomenon in an indirect way, in the form, e.g. of the morphology-density relation.

(ii) For AGN and CTL galaxies, the small-scale environment, as measured by the frequency and luminosity of close neighbours as well as by the tidal parameter $Q$, is very similar. This is suggestive that most of the AGN phenomenon is not due to interactions between the host and its vicinity, but to internal mechanisms like disc/bar instabilities.

(iii) We find an excess of non-circular gas motions in AGN hosts compared with CTL galaxies. Such motions are not associated to AGN feedback and are most likely the result of tidal interactions, possibly associated with the triggering of the AGN.

(iv) We find a correlation between the intensity of the non-circular gas motions in AGN hosts and the strength of the tidal field $Q$, in the sense that the largest values of $\langle \Delta V \rangle$ are found at largest $Q$. This correlation is not found for CTL galaxies. Also, AGN hosts with the most intense radial gas motions present larger tidal fields than their control galaxies. These findings indicate that a fraction of the AGN host in our sample have been triggered by tidal interactions with nearby galaxies.

## ACKNOWLEDGEMENTS

The authors acknowledge support from the Brazilian research agencies CAPES, CNPq, and FAPERGS. GSI acknowledges support from CNPq (142514/2018-7) and FAPESP (Fundação de Amparo à Pesquisa do Estado de São Paulo, Proj. 2022/11799-9). RR acknowledges support from the Fundación Jesús Serra and the Instituto de Astrofísica de Canarias under the Visiting Researcher Programme 2023–2025 agreed between both institutions. RR, also acknowledges support from the ACIISI, Consejería de Economía, Conocimiento y Empleo del Gobierno de Canarias, and the European Regional Development Fund (ERDF) under grant with reference ProID2021010079, and the support through the RAVET project by the grant PID2019-107427GB-C32 from the Spanish Ministry of Science, Innovation and Universities MCIU. This work has also been supported through the IAC project TRACES, which is partially supported through the state budget and the regional budget of the Consejería de Economía, Industria, Comercio y Conocimiento of the Canary Islands Autonomous Community.

Funding for SDSS-III has been provided by the Alfred P. Sloan Foundation, the Participating Institutions, the National Science Foundation, and the U.S. Department of Energy. The SDSS-III web site is http://www.sdss3.org.

SDSS-III is managed by the Astrophysical Research Consortium for the Participating Institutions of the SDSS-III Collaboration including the University of Arizona, the Brazilian Participation Group, Brookhaven National Laboratory, University of Cambridge, University of Florida, the French Participation Group, the German Participation Group, the Instituto de Astrofisica de Canarias, the Michigan State/Notre Dame/JINA Participation Group, Johns

Hopkins University, Lawrence Berkeley National Laboratory, Max Planck Institute for Astrophysics, New Mexico State University, New York University, Ohio State University, Pennsylvania State University, University of Portsmouth, Princeton University, the Spanish Participation Group, University of Tokyo, University of Utah, Vanderbilt University, University of Virginia, University of Washington, and Yale University.

Funding for the Sloan Digital Sky Survey IV has been provided by the Alfred P. Sloan Foundation, the U.S. Department of Energy Office of Science, and the Participating Institutions. SDSS-IV acknowledges support and resources from the Center for High Performance Computing at the University of Utah. The SDSS website is www.sdss4.org.

SDSS-IV is managed by the Astrophysical Research Consortium for the Participating Institutions of the SDSS Collaboration including the Brazilian Participation Group, the Carnegie Institution for Science, Carnegie Mellon University, Center for Astrophysics| Harvard & Smithsonian, the Chilean Participation Group, the French Participation Group, Instituto de Astrofísica de Canarias, The Johns Hopkins University, Kavli Institute for the Physics and Mathematics of the Universe (IPMU)/University of Tokyo, the Korean Participation Group, Lawrence Berkeley National Laboratory, Leibniz Institut für Astrophysik Potsdam (AIP), Max-Planck-Institut für Astronomie (MPIA Heidelberg), Max-Planck-Institut für Astrophysik (MPA Garching), Max-Planck-Institut für Extraterrestrische Physik (MPE), National Astronomical Observatories of China, New Mexico State University, New York University, University of Notre Dame, Observatário Nacional/MCTI, The Ohio State University, Pennsylvania State University, Shanghai Astronomical Observatory, United Kingdom Participation Group, Universidad Nacional Autónoma de México, University of Arizona, University of Colorado Boulder, University of Oxford, University of Portsmouth, University of Utah, University of Virginia, University of Washington, University of Wisconsin, Vanderbilt University, and Yale University.

## DATA AVAILABILITY

No new data have been produced in this work.

## REFERENCES

Alam S. et al., 2015, ApJS, 219, 12
Alonso M. S., Lambas D. G., Tissera P., Coldwell G., 2007, MNRAS, 375, 1017
Araujo B. L. C., Storchi-Bergmann T., Rembold S. B., Kaipper A. L. P., Dall'Agnol de Oliveira B., 2023, MNRAS, 522, 5165
Argudo-Fernández M. et al., 2015, A&A, 578, A110
Baldwin J. A., Phillips M. M., Terlevich R., 1981, PASP, 93, 5
Barnes J. E., Hernquist L. E., 1991, ApJ, 370, L65
Bernhard E., Tadhunter C. N., Pierce J. C. S., Dicken D., Mullaney J. R., Morganti R., Ramos Almeida C., Daddi E., 2022, MNRAS, 512, 86
Boselli A., Gavazzi G., 2006, PASP, 118, 517
Bundy K. et al., 2015, ApJ, 798, 7
Byrne-Mamahit S., Hani M. H., Ellison S. L., Quai S., Patton D. R., 2023, MNRAS, 519, 4966
Cardelli J. A., Clayton G. C., Mathis J. S., 1989, ApJ, 345, 245
Ceccarelli L., Duplancic F., Garcia Lambas D., 2022, MNRAS, 509, 1805
Cid Fernandes R., 2018, MNRAS, 480, 4480
Cid Fernandes R., Mateus A., Sodré L., Stasińska G., Gomes J. M., 2005, MNRAS, 358, 363
Cid Fernandes R., Stasińska G., Schlickmann M. S., Mateus A., Vale Asari N., Schoenell W., Sodré L., 2010, MNRAS, 403, 1036
Coldwell G. V., Lambas D. G., 2006, MNRAS, 371, 786
Darg D. W. et al., 2010, MNRAS, 401, 1552
Deconto-Machado A. et al., 2022, A&A, 659, A131
do Nascimento J. C. et al., 2019, MNRAS, 486, 5075
do Nascimento J. C. et al., 2022, MNRAS, 513, 807
Drory N. et al., 2015, AJ, 149, 77
Duplancic F., Lambas D. G., Alonso S., Coldwell G. V., 2021, MNRAS, 504, 4389
Ellison S. L., Patton D. R., Mendel J. T., Scudder J. M., 2011, MNRAS, 418, 2043
Fischer T. C. et al., 2018, ApJ, 856, 102
Fu H. et al., 2018, ApJ, 856, 93
González Delgado R. M., Cerviño M., Martins L. P., Leitherer C., Hauschildt P. H., 2005, MNRAS, 357, 945
Gordon Y. A. et al., 2018, MNRAS, 475, 4223
Ilha G. S. et al., 2019, MNRAS, 484, 252
Kauffmann G. et al., 2003, MNRAS, 346, 1055
Kauffmann G., Haehnelt M., 2000, MNRAS, 311, 576
Khabiboulline E. T., Steinhardt C. L., Silverman J. D., Ellison S. L., Mendel J. T., Patton D. R., 2014, ApJ, 795, 62
Kim M., Choi Y.-Y., Kim S. S., 2020, MNRAS, 491, 4045
Koulouridis E. et al., 2018, A&A, 620, A20
Krajnović D., Cappellari M., de Zeeuw P. T., Copin Y., 2006, MNRAS, 366, 787
Li W. et al., 2023, ApJ, 944, 168
Liu X., Shen Y., Strauss M. A., 2012, ApJ, 745, 94
Lopes P. A. A., Ribeiro A. L. B., Rembold S. B., 2017, MNRAS, 472, 409
Mallmann N. D. et al., 2018, MNRAS, 478, 5491
Mallmann N. C. Riffel R. 2020, danielrd6/ifscube v1.0 (v1.0). Zenodo. Available at: https://doi.org/10.5281/zenodo.3945237
Mallmann N. D., Riffel R., 2023, ndmallmann/urutau: Urutau. Available at: https://doi.org/10.5281/zenodo.8263936(Accessed 19 August 2023)
Manzer L. H., De Robertis M. M., 2014, ApJ, 788, 140
Menci N., Gatti M., Fiore F., Lamastra A., 2014, A&A, 569, A37
Mountrichas G., Yang G., Buat V., Darvish B., Boquien M., Ni Q., Burgarella D., Ciesla L., 2023, A&A, 675, A137
Noguchi M., 1988, A&A, 203, 259
Osterbrock D. E., 1993, ApJ, 404, 551
Pierce J. C. S. et al., 2023, MNRAS, 522, 1736
Raimundo S. I., Malkan M., Vestergaard M., 2023, Nat. Astron., 7, 463
Rembold S. B. et al., 2017, MNRAS, 472, 4382
Riffel R. et al., 2021, MNRAS, 501, 4064
Riffel R. et al., 2023, MNRAS, 524, 5640
Rogers B., Ferreras I., Kaviraj S., Pasquali A., Sarzi M., 2009, MNRAS, 399, 2172
Ruschel-Dutra D. et al., 2021, MNRAS, 507, 74
Schlegel D. J., Finkbeiner D. P., Davis M., 1998, ApJ, 500, 525
Schmitt H. R., 2001, AJ, 122, 2243
Silva A., Marchesini D., Silverman J. D., Martis N., Iono D., Espada D., Skelton R., 2021, ApJ, 909, 124
Singh A. et al., 2023, ApJ, 953, 64
Storchi-Bergmann T., Schnorr-Müller A., 2019, Nat. Astron., 3, 48
Tempel E., Tuvikene T., Kipper R., Libeskind N. I., 2017, A&A, 602, A100
Thomas D. et al., 2013, MNRAS, 431, 1383
Vazdekis A., Koleva M., Ricciardelli E., Röck B., Falcón-Barroso J., 2016, MNRAS, 463, 3409
Vazdekis A., Sánchez-Blázquez P., Falcón-Barroso J., Cenarro A. J., Beasley M. A., Cardiel N., Gorgas J., Peletier R. F., 2010, MNRAS, 404, 1639
Verley S. et al., 2007, A&A, 472, 121
Wake D. A. et al., 2017, AJ, 154, 86
Yan R. et al., 2016, AJ, 152, 197

This paper has been typeset from a TEX/LATEX file prepared by the author.